

# Algal morphogenesis: modelling interspecific variation in *Micrasterias* with reaction–diffusion patterned catalysis of cell surface growth

David M. Holloway\* and Lionel G. Harrison†

Department of Chemistry, University of British Columbia, 2036 Main Mall, Vancouver, British Columbia, Canada V6T 1Z1

Semi-cell morphogenesis in unicellular desmid algae of the genus *Micrasterias* generates a stellar shape by repeated dichotomous branching of growing tips of the cell surface. The numerous species of the genus display variations of the branching pattern that differ markedly in number of branchings, lobe width and lobe length. We have modelled this morphogenesis, following previous work by D. M. Harrison and M. Kolář, on the assumptions that patterning occurs by chemical reaction–diffusion activity within the plasma membrane, leading to morphological expression by patterned catalysis of the extension of the cell surface. The latter has been simulated in simplified form by two-dimensional computations. Our results indicate that for generation of repeated branchings and for the control of diverse species-specific shapes, the loss of patterning activity and of rapid growth in regions separating the active growing tips is an essential feature. We believe this conclusion to be much more general than the specific details of our model. We discuss the limitations of the model especially in terms of what extra features might be addressed in three-dimensional computation.

**Keywords:** algal development; branching; morphogenesis; *Micrasterias*; patterning; reaction–diffusion

## 1. INTRODUCTION

It is common in plants and fungi for development, with *de novo* pattern formation, to continue throughout the life of the organism. Morphogenesis does not generally occur throughout the organism, but is restricted to small growing regions. Examples include the apical meristems in multicellular plants and the geometrically analogous process of tip growth in cylindrical single cells. Cells of fungal hyphae, root hairs, pollen tubes and some chlorophyte algae elongate by tip growth. Experimental data point to a variety of mechanisms for tip growth (e.g. Steer & Steer 1989; Harold 1990; Green 1994). In some cases, growing tips exhibit branching (sometimes repeated). In unicellular algae, this is common in the order Dasycladales (such as the hair whorls of *Acetabularia*) and is also found in the desmids (the unicellular family of order Zygnematales; Scagel *et al.* 1982).

Desmids are an abundant family, found in fresh water worldwide. A number of genera display tip growth in some aspects of their development. However, repeated branching is most clearly manifest in the genus *Micrasterias* (e.g. see Prescott *et al.* 1977). The stellate form of the fully developed cell is generated by repeated dichotomous branching (figure 1*a–d*). Each branch becomes a growing tip. Much of the marked interspecific variation of form within the genus lies in differences of branch width,

length, total number of branching events (figure 1*e–h*) and branching angle (figure 2*a–c*). In the polar lobe, which usually branches only once (though some species display a small terminal secondary branching), this angle is large (figure 2*c*): between *ca.* 70° and 180°, depending on species. In contrast, the wing lobes have smaller angles: from *ca.* 30° to 60° in the first branching, and down to *ca.* 5° (depending on species) in some subsequent branches.

Experimental data obtained on *Micrasterias* over the past four decades have led to a fairly detailed picture of the cellular biology of morphogenesis (reviewed by Kiermayer 1981). Development starts when the adult cell undergoes mitosis and a septum divides the cell into two daughters. The daughter cells then blow out small bubbles of primary cell wall (figure 1*a*), thought to contain already some rudimentary template for patterned growth (Kiermayer 1964, 1967, 1970*a*). These initial bubbles then grow and undergo the repeated dichotomous branchings that generate the adult form. In the course of 4–5 h, the new semi-cells are completely formed. Shortly after the septum forms, the dictyosomes in the Golgi bodies begin to form a specific type of vesicle, termed the dark vesicles (DV) by Kiermayer (1970*b*). DV are delivered to the plasma membrane and fuse with it (Kiermayer 1970*a,b*), delivering the precursors for primary wall formation, which are largely pectic in nature (Ueda & Yoshioka 1976). In addition, these vesicles deliver membrane with cellulose synthetase rosettes (Giddings *et al.* 1980). These rosettes give rise to a microfibril of fixed length in the wall, so the extension of wall is always directly related to extension of membrane (Stachelin & Giddings 1982).

\* Author for correspondence (lionel@pepe.chem.ubc.ca).

† Present address: Mathematics Department, British Columbia Institute of Technology, 3700 Willingdon Avenue, Burnaby, British Columbia, Canada V5G 3H2.

Disruption of vesicle secretion leads to cessation of cell growth (Hoftberger *et al.* 1995).

Vesicle fusion with the plasma membrane occurs in a patterned manner. This was first demonstrated by reduced-turgor experiments (Kiermayer 1964; Tippit & Pickett-Heaps 1974; Ueda & Yoshioka 1976). With the pressure reduction, the cell surface ceases to extend, but wall material continues to be delivered and accumulates on the inside of the plasma membrane. Accumulation is heaviest at the growing tips, and clearly reflects the morphogenetic pattern. Fluorescent labelling of  $\text{Ca}^{2+}$  in the plasma membrane by the chelate chlorotetracycline (CTC) shows a very clear spatial pattern, with highest  $\text{Ca}^{2+}$  on the growing tips (Meindl 1982). This is in accord with the role of  $\text{Ca}^{2+}$  in fusion of vesicles to the plasma membrane (Gratzl 1980; Steer 1988; Battey & Blackburn 1993). The  $\text{Ca}^{2+}$  patterns observed by CTC coincide with the measured ionic currents, which flow in at lobe tips and out in clefts (Troxell 1989; Troxell & Scheffey 1991; Troxell *et al.* 1986). It has recently been shown that  $\text{Ca}^{2+}$  patterning is indeed limited to the plasma membrane, or at the most to a very thin submembrane layer. Using microinjection of the free (as opposed to membrane-bound)  $\text{Ca}^{2+}$  chelate fura-2, Holzinger *et al.* (1995) found no cytoplasmic gradients of  $\text{Ca}^{2+}$ .

Cytoplasmic streaming is a necessary component of the morphogenesis. Streaming apparently occurs along actin microfilaments. Disruption of these by cytochalasin B inhibits normal development (Ueda & Noguchi 1988). These authors found that microfilaments always extend into growing tips (and from adult semi-cell to developing semi-cell through the isthmus), and suggested that they may be bound to plasma membrane proteins. They argue for a passive role for microfilaments in morphogenesis. Normal microfilament activity in turgor-reduced cells does not give normal morphogenesis (this is in strong contrast with fungal hyphae; Harold *et al.* 1995), and microfilament arrays are not known to be able to branch to provide the driving force for tip branching. Several studies have found morphological effects from extracellular  $\text{Ca}^{2+}$  inhibition or disruption of normal  $\text{Ca}^{2+}$  transport across the plasma membrane (Lehtonen 1984; McNally *et al.* 1983). These effects are thought to involve disruption of  $\text{Ca}^{2+}$  control of actin function. In contrast, disruption of microtubule assembly by colchicine has long been known to have no detectable effect on morphogenesis (Kiermayer 1968).

To summarize, vesicle formation in the Golgi and transport via microfilaments to the plasma membrane are required components of cell surface growth, but do not contain the mechanism for dichotomous branching. There appears to be consensus in the experimental literature that patterned surface extension is controlled in the plasma membrane. This view is supported by the visualized patterns of membrane bound  $\text{Ca}^{2+}$  and by the role  $\text{Ca}^{2+}$  plays in many systems in fusing vesicles with the plasma membrane. Kiermayer & Meindl (1989, fig. 13) have proposed that it is a  $\text{Ca}^{2+}$ -binding membrane protein which controls the vesicle recognition and fusion process.

In the present work, which continues that reported by Harrison & Kolář (1988), we use a model in which the principal pattern generator is a two-morphogen reaction–diffusion model (Turing 1952). We do not regard this as the

only possible type of pattern generator. It is just one convenient choice to explore the necessary features of cell surface growth with a reliable mechanism to generate membrane pattern. As it turns out, the Turing mechanism is robust and versatile enough to model the developmental sequences observed in diverse species. We identify the Turing morphogens with non-uniformly distributed membrane-bound molecules, one of which catalyses extension of the plasmalemma (perhaps the  $\text{Ca}^{2+}$ -binding protein of Kiermayer & Meindl (1989)). Suppose, then, that a two-peak distribution of this catalyst has been produced at a tip that is actively growing. What mix of growth and tip boundary control will interpret this catalyst pattern so that the tip splits into two parts, each of which will become a cylinder itself elongating by tip growth?

This question points to a peculiarity of tip growth that, to our minds, has not yet been adequately addressed in the literature. A catalyst maximum can result in a dome-shaped tip on a progressively elongating cylinder as long as the actively growing tip region is self-limiting, i.e. it must pull its boundary up after itself (Green & King 1966). Branching tip growth will result from a splitting of the original catalyst maximum only if new boundaries are drawn around each new catalyst maximum. Harrison & Kolář (1988) found that catalyst peak-splitting would not generate repeated dichotomous branching without complementary formation of morphogenetically ‘dead’ regions between catalyst maxima. Such feedback between patterning mechanism and pattern boundaries has also been discussed for branching tip growth in *Acetabularia* (Harrison *et al.* 1988; Harrison 1992). We use a new model for feedback of the chemical patterning on its boundaries in the present work. The parameters controlling this feedback (rate constants and concentration thresholds) have a strong effect on branching angle, lobe width and lobe length. Such control has allowed us to make a start on modelling species-specific variations on the basic *Micrasterias* shape. Finding interspecific differences in the kinetic parameters of the morphogenetic process may point us towards the genetic differences that delineate species and must ultimately be the cause of these parameter differences.

## 2. PRINCIPAL FEATURES OF THE MODELLING

In this section, our modelling strategy is described in general terms. In §3, the details of the putative chemistry, growth algorithm and computational methods are given.

### (a) *The chemical patterning mechanism*

Whenever pattern advances to greater complexity, as in the onset of dichotomous branching, one must seek a crucial control step without which the increase in complexity would not occur. In our modelling, we postulate that this control step is a chemical reaction mechanism between molecular species in the cell membrane. The minimal complexity of reaction mechanism that will generate complex spatial distributions of chemical concentrations was defined by Turing (1952). It requires catalytic and inhibitory interactions between two substances (morphogens)  $X$  and  $Y$ ; and both must diffuse, but at different rates. These substances are reaction intermediates, and one may need to consider the reactants ( $A$ ,  $B$ , etc.) from which they are formed. In this

work (§3) we chose one of the numerous later elaborations of reaction–diffusion theory, the Brusselator of Prigogine & Lefever (1968). This model, unlike some others, responds very well to increase in size of a system by generating increasing complexity of chemical pattern. We postulate that morphogen  $X$  is a catalyst for cell membrane extension, and that control of the boundaries of growing tips is achieved by feedback from  $X$  into the supply of reactant  $A$  (§2c(i); §3, equations (4) and (5)).

The property of adaptability to size increase is not unique to the Brusselator. A larger class of reaction–diffusion models, including variants of the Brusselator (Tyson & Light 1973; Tyson & Kauffman 1975; Sel'kov (1968) with added diffusion terms, see Harrison & Lacalli (1993)), might be equally suitable. This is an obstacle in trying to connect the patterning process back to its genetic origins, because the lines of communication (i.e. the postulated reaction mechanisms) would not be precisely the same for different models.

### (b) Dimensionality in the modelling

The development of a *Micrasterias* cell takes place in a three-dimensional (3D) space (figure 1e–h). The dichotomous branchings and ensuing tip growth (figure 1, especially f) are coordinated, usually, so that all lobes are in the same plane. Because of this geometry, the outline of the cell can be drawn in a two-dimensional (2D) space. Since computations in 3D are very time consuming and require relatticing procedures (for the mesh representing the surface), which are cumbersome and difficult to devise, it is an advantage if computations can be reduced to 2D. We needed to carry out a large number of computations quickly, to determine the effects of changing various parameter values. How may the growth algorithms be reduced to 2D, while still retaining the essential features which allow study of chemically driven morphological change?

There are two obvious methods to consider.

- (i) Approximate the cell as a flat sheet which grows at the edge like a 2D crystal. In this case, growth occurs because material is added directly on to the edge, and the direction of growth is determined by the direction that material is added, i.e. growth is generally normal to the edge (e.g. see Denet 1996). This approximation seems most reasonable for species with broad flat lobes such as *M. rotata* or *M. verrucosa* (figure 1e), but is less applicable to species with rounded lobes, such as *M. radiata* or *M. tropica* (figure 1f,h).
- (ii) Approximate the growth as confined to a line, the outline of the growing semi-cell. As seen in figure 1e–h, the cell does indeed narrow to a very thin growing edge. In accord with the experimental evidence for vesicle fusion, outward movement of this edge occurs because of tangential increase in the length of the line. Though the experimental system is 3D, the 2D treatment can capture, with some limitation, the essential connection between surface increase and outward movement. This approach was therefore the one adopted by Harrison & Kolář (1988) to study the changing morphology of a closed loop growing as specified by the chemically

patterned catalyst  $X$ . The same strategy is used in the present work, with the simple growth and relatticing algorithms described in §3.

There is one obvious feature of *Micrasterias* development that cannot be tackled in a 2D computation. In-plane branching is a common feature of most species, but in the present work this has been forced on the system by the reduction in dimensionality. In some species, *Micrasterias* displays branchings in two mutually perpendicular planes (figure 3a). A preliminary 3D computation by Kolář begins to address these cases: it shows a dichotomous branch and an  $X$ -distribution within each branch that will lead to an out-of-plane branching at the next event (Harrison 1992, fig. 3).

A less obvious limitation on the validity of 2D computations concerns the contrast between lobe tips (T) and the clefts (C) between lobes (figure 3b). The solid outline is the 2D representation. It can obviously be regarded as a planar section of the 3D cell surface. In the region of the lobe tips, tangential area increase in 3D can lead to outward movement of the surface; and the 2D representation can show the same property. This is method (ii) above. But the outward movements of the clefts C, which are saddle points on the surface, are constrained in directions such as CS (section in a plane perpendicular to that of the diagram) in a way that cannot be taken into account precisely by 2D work on the solid outline alone. In 3D computations, the effects of this geometry would be taken into account automatically. For instance, the section CS, seen in the plane of the section, looks like a cross-section of a tip; slow (or zero) growth of this ‘tip’ will constrain cleft C not to move outwards quickly (or at all). In 2D computations, this constraint is absent, and a condition to represent it has to be introduced artificially.

### (c) Boundary control and directionality in branching tip growth

Simple tip growth elongates a cylinder. The boundary of the growing tip is a circle, and the direction of elongation is perpendicular to the plane of that circle. When the growth catalyst pattern on the plasmalemma changes from a single maximum to two (or more) maxima, the resulting branching growth is not defined as tip growth until the two (or more) new boundaries have been drawn. Harrison & Kolář (1988) showed this in 2D computations: in the absence of such boundary respecification, repeated splitting of morphogen peaks did not lead to repeated dichotomous branching in the cell surface. The feedback of the patterning mechanism into the boundaries is therefore a crucial feature of any model of cell surface growth. With such feedback Harrison & Kolář (1988) were able to model the morphological expression of repeated dichotomous branching in the patterning mechanism (figure 2d,e). When new boundaries are drawn in 3D they will most probably (though not necessarily) be planar, and the new growth directions will be perpendicular to these planes. In 2D, the boundaries are not circles, but two points on either side of the new growth maximum. The direction of growth will be roughly perpendicular to the line joining these points (figure 4b–e). Thus, the branching angle strongly depends

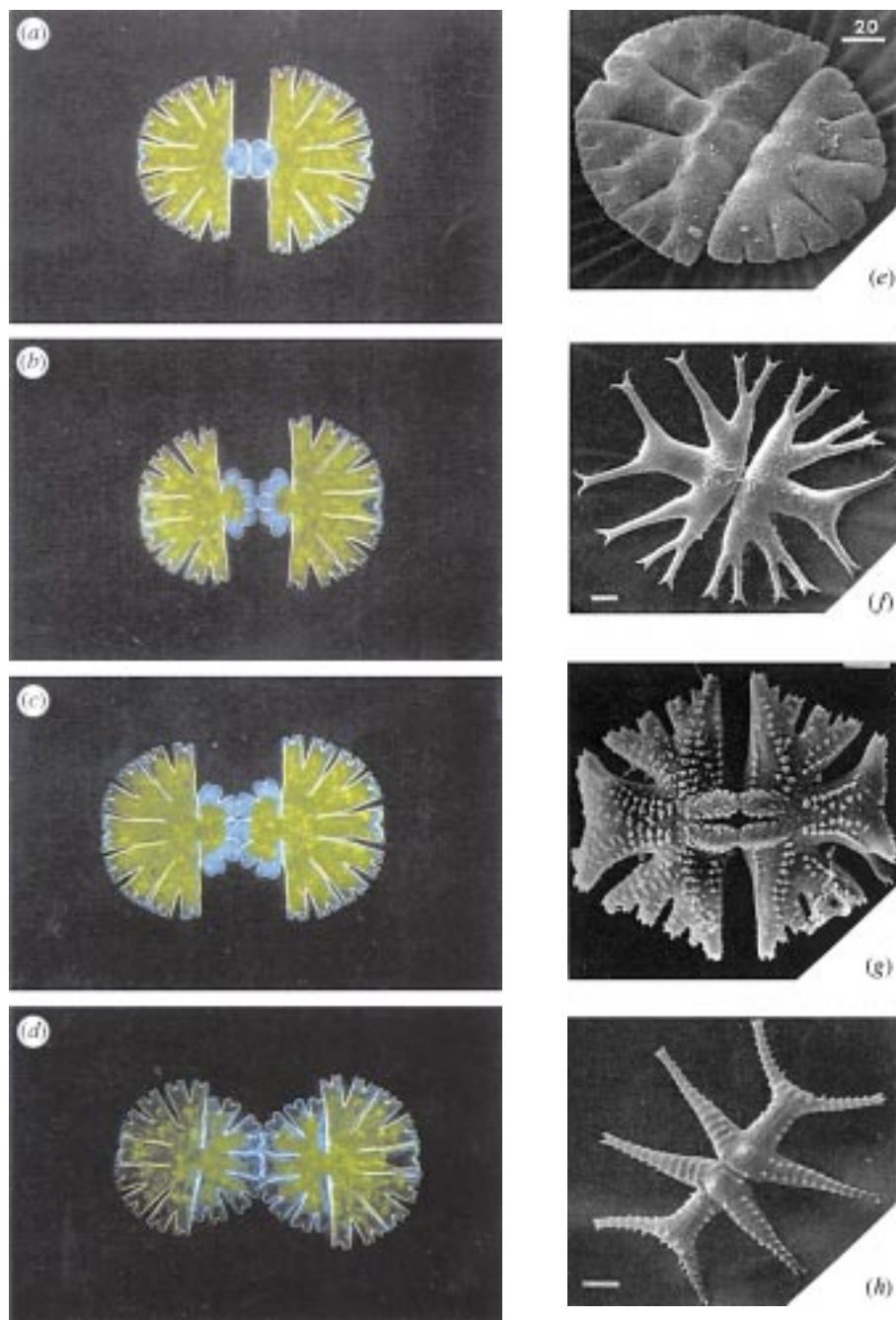


Figure 1. (a–d) Semi-cell morphogenesis in two daughter cells following mitosis in *Micrasterias thomasiana*, roughly 1, 2, 3 and 4 h stages, from Harrison (1994) with permission. (e–h) From Couté & Tell (1981) with permission, SEMs of fully formed cells illustrating diversity of form in the genus: (e) *M. verrucosa* var. *verrucosa*; (f) *M. radiata* var. *brasiliensis*; (g) *M. americana* var. *bimamillata*; (h) *M. tropica* var. *senegalensis*. The bars indicate 20  $\mu\text{m}$  in (e), 10  $\mu\text{m}$  in (f–h).

on the mechanism that draws the new boundaries. So, not only is the presence of such a mechanism crucial, but the details of it are very important in determining the expressed morphology.

#### (i) *Boundary-creating mechanism*

In the idealized model of tip growth that is the basis of our 2D computations, there is neither chemical patterning nor morphological growth in the region beyond the boundary of a morphogenetic region. We specify the no-growth condition by locking points in place once they are in such a region. This approximation does not correspond precisely to experimental evidence. In fact, slow outward movement continues in clefts. In the case of *M. rotata*, Harrison & Lacalli (1978) tried to estimate 'growth trajectories' for various points on the cell outline. They concluded that the outward advance of the clefts was at

about one-half the rate of the lobe tips. The boundaries in *Micrasterias* development (and in other instances of algal tip growth, such as *Acetabularia* development) are actually between fast-growing pattern-forming regions and slow-growing unpatterned regions. For the reasons discussed above in relation to figure 3b, it is difficult to program the slow growth properly in the 2D approximation.

Boundary formation requires an addition to the chemical pattern-forming mechanism. Such a mechanism (§3a, equations (1) and (2)) normally contains several parameters such as reactant concentrations ( $A$ ,  $B$ ), rate constants ( $a$ ,  $b$ ,  $c$ ,  $d$ ) and diffusivities ( $D_x$ ,  $D_y$ ). If the values of these remain fixed, the mechanism retains pattern-forming ability no matter how low the concentration of morphogen  $X$  becomes in any region. Therefore, a mechanism to cause the collapse of morphogenesis must change the value of at least one of these parameters. The

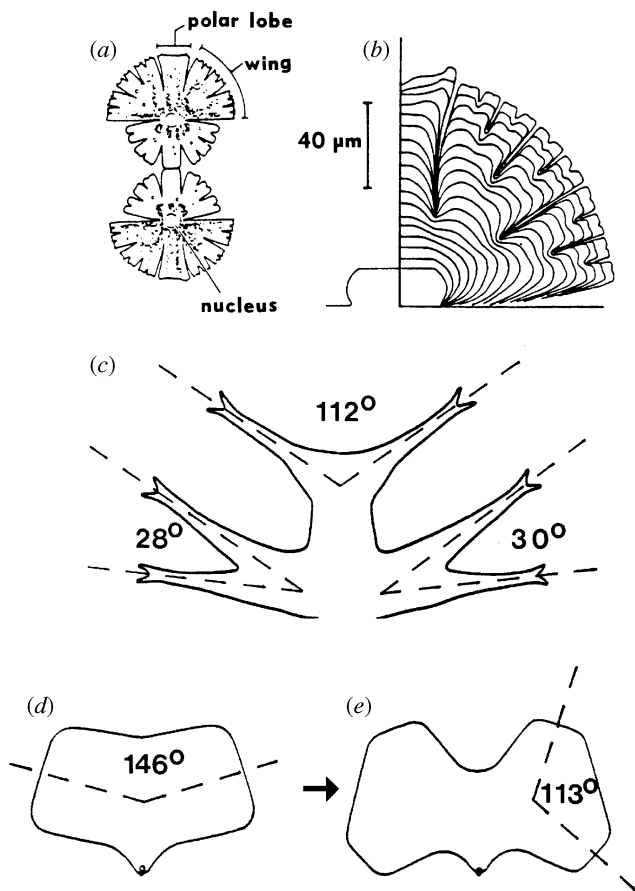


Figure 2. (a) *M. rotata*, sketch of 3 h stage. Polar and wing lobes labelled on old semi-cell. (b) *M. rotata*, growth profiles at 10 min intervals, 20 °C. (a,b) are from Lacalli & Harrison (1987) with permission. (c) Typical contrast of polar and wing lobe branching angles: fully formed semi-cell outline of *M. radiata* var. *radiata* f. *radiata* from Prescott *et al.* (1977) with permission. (d,e) Two stages from a computation of Harrison & Kolář (1988), with permission, showing branching angles for first and second dichotomous branch when the 'age effect' was used to limit and separate morphogenetic regions.

most obvious feedback scheme is for low  $X$  to interfere with the supply of reactant  $A$  or  $B$ .

Two such mechanisms have been used in 2D *Micrasterias* computations. Harrison & Kolář (1988) used a technique, termed the 'age effect', that cut off the  $A$  supply wherever growth had been slow for some time. This was not envisaged as a mechanical change in the rigidity of the cell wall, but as a change in chemical reactivities at the plasma membrane. Newly added membrane was given age zero, and thereafter aged in real time. Thus rejuvenation was most effective at the fast growing lobe tips. The clefts between the lobes were the oldest. Supply of reactant  $A$  was reduced linearly with age to zero at a particular threshold age, rendering that region morphogenetically inactive. This mechanism, however, has limited ability to control branching angles. Therefore, we have developed a new (though related) mechanism. The boundaries are created when the growth catalyst,  $X$ , drops below a threshold value,  $X_{th}$ . At this point, morphogenesis is shut off, and no growth is allowed. The details of this mechanism, and how it provides for a wider range of branching angles, will be discussed below.

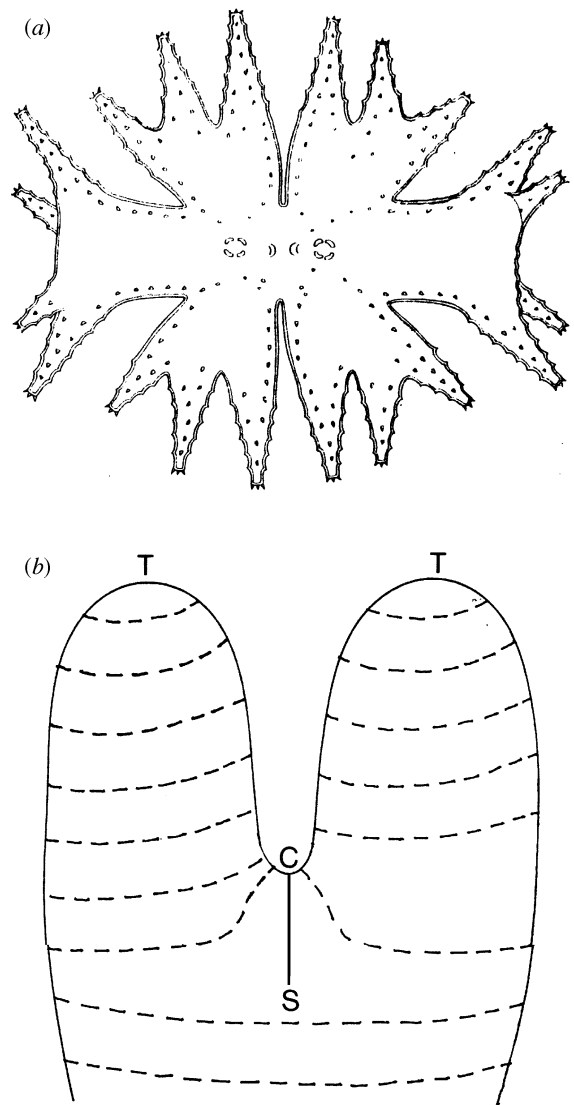


Figure 3. Features requiring 3D computations. (a) Out-of-plane branching of polar lobes of *M. mahabuleshwariensis* var. *Wallichii* from West & West (1905). (b) Diagrammatic sketch of tips T and cleft C, showing that the 2D approximation (solid line) may be expected to give a good account of growth near T but not near C. The solid line CS is intended to suggest a section through the cell surface in a plane perpendicular to that of the diagram.

#### (ii) Control of the branching angle

The 'age effect' model was found to generate only obtuse branching angles. For three stages of sequential branching, the branches first appear at about 115° to each other (second stage, figure 2e). As they extend, this angle increases to 130–150° (first stage, figure 2d). Such values are quite common for the single branching of the polar lobe in various species of *Micrasterias*. The model would not, however, generate the acute branching angles typical of the wing lobes.

The branching angle problem is illustrated, in the 2D approximation, in figure 4. Generation of a double peak pattern of the growth catalyst  $X$  on a rounded tip (figure 4a) will lead to flattening of the tip (figure 4b). (Such flattening of the growing tip prior to branching has been well documented in *Acetabularia*; e.g. Harrison *et al.* 1981.) For most reaction–diffusion mechanisms, this morphological

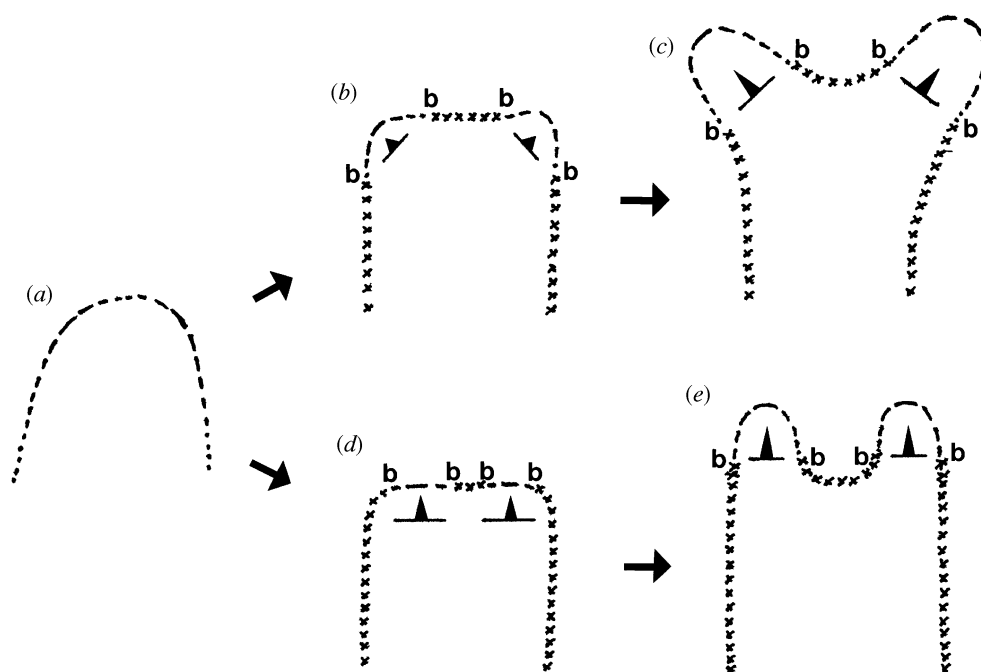


Figure 4. Sketches of tip shapes and  $X$  morphogen distributions to illustrate the branching angle problem (see text). Boundaries between active and 'dead' regions are marked  $b$ .  $\times \times \times$  morphogenetically 'dead' region;  $\cdots$  low  $X$  concentration;  $---$  high  $X$  concentration. Arrows are growth directions, normal to the line joining two boundary points.

change will leave the growth maxima centred on the corners, leading to a high branching angle (figure 4*b,c*). For a low branching angle, the growth maxima must be pushed up on to the flat region of the tip (figure 4*d,e*). We were not able to achieve this using the 'age effect'. In this work, we have successfully modelled acute branching angles with our more direct chemical kinetic formulation of a feedback from  $X$  into production of  $A$  (§ 3*c*). This acts much more quickly than the 'age effect', and hence is more versatile in its effects and responsive to parameter changes. For instance, a sequence like that sketched in figure 4*d,e* is established as follows. A rather slow splitting of the  $X$  peak, allowing formation of a flattened tip, is followed by quick establishment of a small 'dead' region between the two new peaks. This, together with a rapid drain-off of  $X$  to destruction in the flanking 'dead' regions, tends to anchor the two new growing tips on top of the flattened tip and allow progress to low-angle branching.

#### (d) *Changes in parameter values with position and time*

A model is most complete if parameter variations (along either position in the system or time in the developmental progression) necessary for morphogenesis are themselves accounted for by dynamic mechanisms. If this can be done, the total parameter set in the computer program will contain only constant values. In the present work, three different parameter variations have been introduced without dynamic models to generate them.

- (i) The earliest morphology of the *Micrasterias* semi-cell is a three-lobed shape, of which the central, polar lobe will branch only once, and the lateral, wing lobes will go on to branch from zero to five times (depending on species). (The final very small branching is not counted in these numbers.) This early morphology is believed to result from a patterning template established at septum formation (Kiermayer 1964, 1967, 1970*a*). In our model, the three-lobe pattern is specified by an initial gradient in the reactant  $A$ . To account for the different degree

of branching between pole and wings, one kinetic parameter ( $k_p$ , see § 3, equation (5)) is changed by roughly 5% between these two regions.

- (ii) It is known experimentally for the morphogenesis of *M. rotata* (Lacalli & Harrison 1987) that successive branchings of the wing lobe occur on a decreasing spatial scale. This decrease was a factor of about 2.5 from the first to the fourth branch. To match these data, we arbitrarily changed the values of parameters controlling the spacing of the  $X$  peaks over time in our computations.
- (iii) Harrison & Kolář (1988) found that closed loops either with simple tip growth or with branching could be generated, depending on the initial value of reactant concentration  $A$ . In our work, the corresponding control parameter is the threshold value of  $X$  for cessation of morphogenesis,  $X_{th}$ . We have found computation with a constant value of this parameter sufficient for modelling species which display zero or single branching. However, for higher branching order (while maintaining acute angles), it is necessary to switch this parameter between tip growth and branching values *during* the computation. It is possible that there exists a mechanism within the cell to control the timing of branching.

### 3. MODELS AND METHODS

To model *Micrasterias* morphogenesis as an extension in cell surface driven by chemical pattern in the plasma membrane, the computations have two major components: a model for the chemical patterning and a model for the growing surface.

#### (a) *The chemical patterning mechanism*

As discussed in § 2*a*, the simplest mechanism for generating periodic chemical pattern is reaction-diffusion, as first described by Turing (1952). We use a specific reaction-diffusion model, the Brusselator (Prigogine & Lefever 1968), which tends to create very regular pattern, in contrast to other models (e.g.

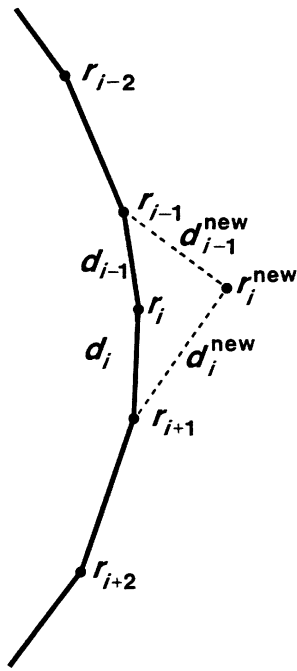
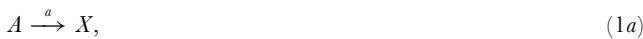


Figure 5. Geometrical basis of the 2D growth algorithm (see text). From Harrison & Kolář (1988), with permission.

Holloway & Harrison 1995). This model consists of the following reaction scheme



$X$  and  $Y$  are reaction intermediates; both diffuse, and  $X$  is the growth catalyst.  $A$  and  $B$  are the reactants.  $D$  and  $E$  are products, which nowhere have to be used in the modelling. The following equations give the time rate of change of  $X$  and  $Y$ , including both reaction and diffusion, at every point on the surface

$$\frac{\partial X}{\partial t} = aA - bBX + cX^2Y - dX + D_X \nabla^2 X, \quad (2a)$$

$$\frac{\partial Y}{\partial t} = bBX - cX^2Y + D_Y \nabla^2 Y, \quad (2b)$$

where the terms with Laplacian operator  $\nabla^2$  represent diffusion ( $D_X$  and  $D_Y$  are the diffusivities of  $X$  and  $Y$ ). These equations have not been solved analytically (by pen and paper) for long-time behaviour on a growing spatial domain; study of this requires computation. To program these equations into the computer, they must be discretized in time and space, i.e. changes in  $X$  and  $Y$  are calculated at multiples of a finite time-step,  $\Delta t$ , and at a finite set of points,  $r_i$ , that represent positions on the outline of the growing semi-cell (figure 5, and §2b).  $r_i$  and  $r_{i+1}$  are separated by distance  $d_i$ , a discrete line segment in the outline.

In all computations, the initial shape was a semicircle, radius 150 distance units, representing a semi-cell about 30 min after

mitosis, before lobe differentiation. This was approximated in the computer by 121 points,  $r_i$ . Values of rate constants and reactant concentrations were always  $a=0.01$ ,  $b=1.5$ ,  $c=1.8$ ,  $d=0.07$ ,  $A(\text{initial})=5.5-4.4$ ,  $B=1.0$  and diffusivity ratio  $D_Y/D_X=10.0$ . These values are in an appropriate region of parameter space for pattern formation (Harrison 1993) and were used for *Micrasterias* morphogenesis by Harrison & Kolář (1988). (As indicated in §2d,  $A$  was initiated in a small amplitude three-peak pattern. This was three cycles of a cosine pattern. The stated limits for  $A(\text{initial})$  are its maximum and minimum.) From these values, for maximum  $A(\text{initial})$  the homogeneous steady state concentrations of the morphogens (Harrison 1993, p.269) are  $X_0=aA/d=0.7857$  and  $Y_0=(bd/ac)(B/A)=1.0606$ . At  $t=0$ ,  $X$  and  $Y$  are initialized as  $X_0$  and  $Y_0$  at every point  $r_i$ . Noise is added to simulate concentration fluctuations. The noise is scaled to  $1/\mathcal{N}^{1/2}$ , the standard deviation of a Poisson distribution, where  $\mathcal{N}$  is the number of molecules per point. We assume  $\mathcal{N}=10\,000$  to correspond to unit value of  $X$  or  $Y$ . The noise is thus of order 1% of  $X_0$  or  $Y_0$ , since these are both close to unity.

Starting with  $X$  and  $Y$  values at  $t$ , new values at  $t+\Delta t$  are calculated from these. (This is known as forward-differencing, the simplest computational method.) Each such step is an iteration, and is repeated several hundred thousand times for each computation. To avoid an instability, the time-step must be kept small ( $\Delta t \leq (d_i)^2/2D$ ; the value 0.005 was used in all our computations). An alternative approach, backward-differencing, does not have this instability and can potentially be faster, by allowing use of a larger  $\Delta t$ . However, we found, by computation, that the growth algorithm (described below) has an instability which imposes a more stringent constraint on  $\Delta t$  than does the solution of the reaction-diffusion equations. Therefore, there is no purpose in using a more computationally intensive backward-differencing scheme. Emergence of a recognizably periodic pattern of  $X$  and  $Y$  from initial conditions takes a few tens of thousands of iterations.

### (b) Cell surface growth

This pattern is translated into surface growth by the following change in the  $d_i$  per time-step, which depends on the  $X_i$ :

$$\Delta(d_i)/\Delta t = c_g d_i (X_i + X_{i+1})/2, \quad (3)$$

where  $c_g$  is the growth rate constant. For constant  $X$ s this equation would represent exponential growth of  $d_i$ .  $X$  concentration is defined at the  $r_i$  on the ends of the  $d_i$  segment, so an average value is used. Every time-step, the  $d_i$  grow according to equation (3) and new  $r_i$  are calculated as the intersection of the new  $d_i$  radii (figure 5). The outward intersection is always chosen: we presume that turgor pressure assures this for the living cell. When the  $X_i$  on each side of a  $d_i$  drop below a threshold value,  $X_{th}$ , growth of  $d_i$  ceases. In addition, when this occurs change in the position  $r_i$  is no longer computed: the point becomes fixed. Over time,  $X$ -patterning will make the  $d_i$  unequal, so care must be taken to use the proper  $d_i$  for the exchange of material between any two points in the diffusion calculation (see Harrison & Kolář 1988).

Accuracy of both the reaction-diffusion solution and the computed shape depends on the spatial steps and the time-step. Accuracy was tested in several computations by halving the time-step and decreasing the spatial steps. This did not significantly change the computed shape, suggesting that the steps were small enough for finite differencing to give a good account of continuum behaviour. To maintain accuracy throughout a

computation as the  $\mathbf{d}_i$  grow, a new point is inserted at the midpoint of a  $\mathbf{d}_i$  as soon as that segment has exceeded twice its original length.

**(c) Feedback from  $X$  to  $A$ , and threshold  $X$**

The feedback from morphogen  $X$  into reactant  $A$ , necessary for generating acute branching angles, was modelled as the following chemistry (in addition to equations (1)).



$S$  is a substrate,  $F$  is a product formed by the decay of  $A$ , and  $k_p$  and  $k_d$  are rate constants. From equations (1a) and (4), the rate equation for  $A$  is:

$$\partial A / \partial t = k_p S X - k_d A^2 - aA. \quad (5)$$

The second-order decay of  $A$  is necessary for maintaining self-regulation of the  $X$ - $A$  feedback loop: concentration explosions occur with a linear decay. Addition of equation (5) to equations (2) allows for squared off peaks with slow branching if the proper parameter values are chosen. In particular, it is necessary for  $k_p \gg k_d$  to generate acute branching angles (the specific ratio depends on the values of the other kinetic parameters in equations (2)). This maintains the square peaks: if  $k_p$  is too low, then the peaks are sharp and split quickly, leading to obtuse angles. If  $k_p$  is too high, the morphogen peaks become very square, and the reaction-diffusion mechanism often fails to respond to growth by peak-splitting. With the  $A$ -feedback of the present model, we are able to move from rounded to square peaks by changing only the parameter  $k_p$ . In all computations,  $k_d = 0.15$ .

For  $X \leq X_{th}$ , equations (2) and (5) are replaced by

$$\partial X / \partial t = -n_d X + D_X \nabla^2 X, \quad (6a)$$

$$\partial Y / \partial t = D_Y \nabla^2 Y, \quad (6b)$$

$$\partial A / \partial t = 0; \quad (6c)$$

and the growth of the cell surface ceases:

$$\partial \mathbf{d}_i / \partial t = 0. \quad (6d)$$

These conditions create regions that are 'dead' for both chemical patterning and cell surface extension. Within these regions,  $X$  is decaying, usually very rapidly ( $n_d > 1$ ). Both  $X$  and  $Y$  can diffuse within the dead regions and cross their boundaries. Thus the dead regions can act as a sink for morphogens moving from the morphogenetic regions.

As discussed in §2d, three arbitrary parameter variations have been used. First, variation between the polar lobe and the wing lobes within one species has been modelled by a spatial variation of  $k_p$ . Modelling of different species may require different ratios of  $k_p$  in the two regions. Second, when modelling semi-cells with two or more branchings in the wing lobes, one must take into account the decrease in spacing observed by Lacalli & Harrison (1987). Otherwise, significant lobe overlap results as branching progresses and lobe number increases. This decrease in spacing may arise from decrease of a chemical rate over time. However, within our model, the rate parameters are too tightly constrained by the requirements of controlling lobe shape and branching angles to be available for decrease over

time. In reaction-diffusion, the diffusivities  $D_X$  and  $D_Y$  can also control the spacing. Therefore, we decrease these (while maintaining their ratio,  $D_Y/D_X$ , constant) by multiplying them at each iteration by a factor slightly smaller than one, such that they halve the spacing every 250 000 iterations. Finally, the differences in branching order between species, and to some degree the differences in lobe shape, can be modelled by shifting  $X_{th}$  at specific times during a computation. In general, low  $X_{th}$  produces branching, while high  $X_{th}$  maintains tip growth. The reason for this is that high  $X_{th}$  moves the tip boundary up quickly and keeps the tip small; but low  $X_{th}$  lets the tip become bigger, so that the chemical pattern on the tip splits. By shifting between regimes of low and high  $X_{th}$ , successive acute-angled branches can be generated. The values of  $X_{th}$  are constrained, however, by other parameters in the model, most notably the growth rate,  $c_g$ . Therefore, it is the timing of  $X_{th}$  shifting between low and high that gives an independent control on branching events. We have found this control to be necessary for generating higher-branching *Micrasterias* morphologies. This timing control may be provided by signals within the cell.

**(d) Noise and random errors**

With this model, it is difficult to reduce the effects of random errors sufficiently to match the degree of symmetry often found in *Micrasterias* morphology (but see figure 10c for asymmetries in natural populations). This problem has two components. First, there is some error due to the finite nature of the grid, the set of points  $r$ . Any irregularity in the distribution of these can lead to asymmetry in the branching. Second, slight asymmetries in the morphogen distributions tend to get amplified because of the interaction between chemical pattern and growth. Several steps were taken to smooth this. First, we used a model, the Brusselator, which tends to give very symmetrical pattern. Second, though noise is not necessary to initiate formation of the three-peak pattern, because it is built into initial  $A$ , nevertheless approximately 1% noise (see §3a) was added to  $X$  and  $Y$ , usually for each of the first 10 000 iterations, to simulate fluctuations. (For later addition of noise see §4c). Reaction-diffusion without growth was allowed until 100 000 iterations in order to smooth this early pattern. Even after growth begins, the reaction-diffusion remains on a faster time-scale than the growth. We computed between 500 and 1000 reaction-diffusion iterations per growth iteration (depending on the growth rate constant,  $c_g$ ). This gives time for the chemical pattern to adjust after each shift in the surface.

Computations were carried out on a Silicon Graphics Iris Indigo workstation with a MIPS R3000A processor running IRIX. Programs were written in C and visualized with routines written in the Silicon Graphics Graphics Library.

## 4. RESULTS

With 2D modelling, we have been able to generate a number of features of *Micrasterias* morphology. These include general features, such as acutely angled wing branches, and species specific features, such as branching number and lobe width. The requirements for tip growth and acute branching angles strongly constrain the reaction parameters in the model. Independent variables, such as the spatial distribution of  $k_p$  and the timing of  $X_{th}$ -shifting, are necessary for generating interspecific variation. The common parameters, used in all computations, are given in §3a. The computations will be presented in

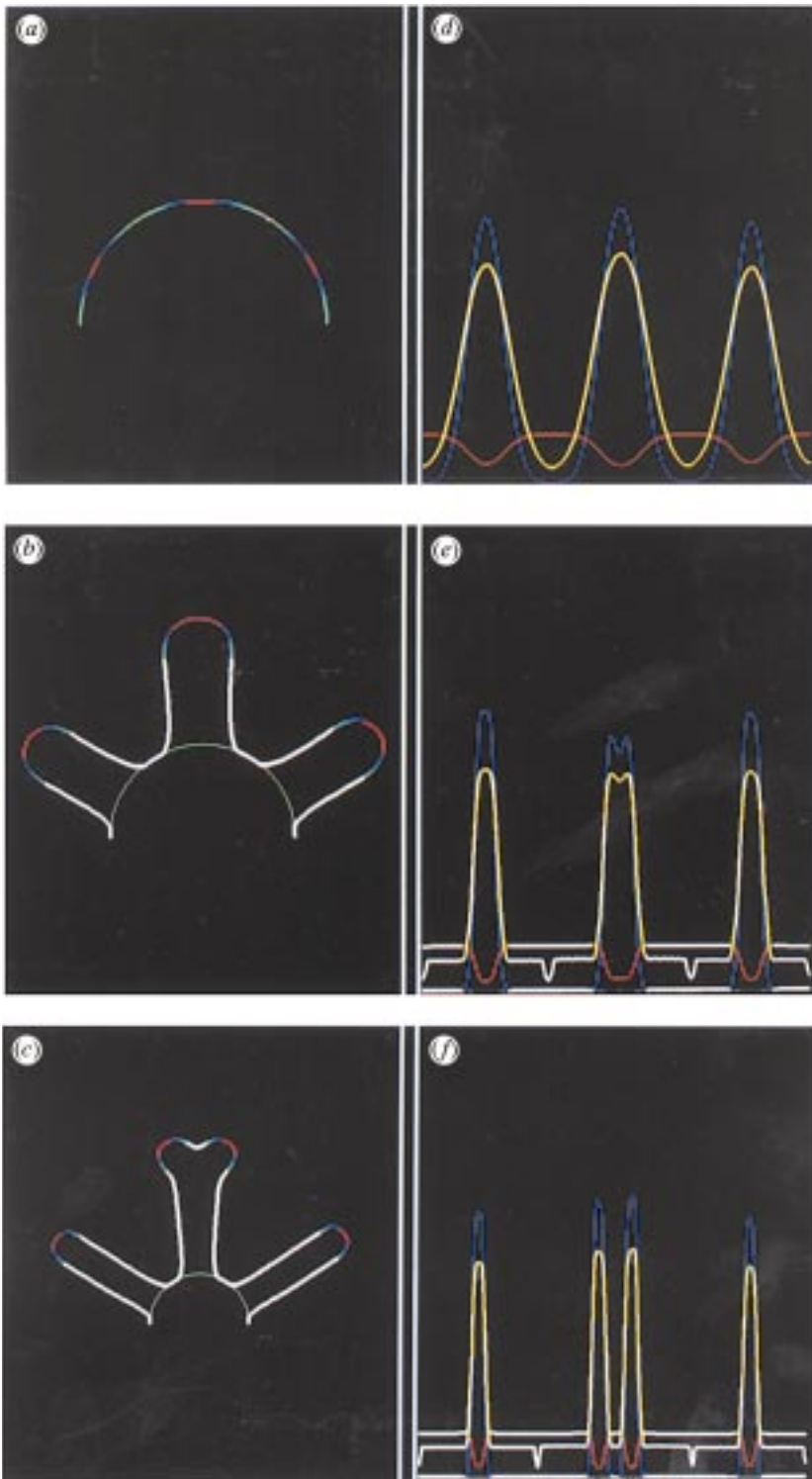


Figure 6. Computation of shape development of a *Micrasterias* semi-cell with no branching in the wing lobes. (a) The initial semicircular shape. (b,c) Later stages, with the initial semicircle repeated (green) to show scale change. Cell outline colour-coded for  $X$  morphogen concentration: yellow  $>$  red  $>$  blue  $>$  green; white for 'dead' regions,  $X < X_{th}$ . (d,e,f) Concentration plots for stages (a,b,c) respectively. Abscissae: distance along cell outline. Ordinates: concentrations of  $X$  (blue),  $Y$  (red); and  $A$  (yellow). 'Dead' regions white. Iterations: (a): 100 000; (b): 160 000; (c): 220 000.

order of increasing wing branching number, followed by computations on abnormal development. A table for the specific parameters of individual computations will be presented in each subsection.

#### (a) Zero-branching wing lobes

Figure 6 shows a computed developmental sequence of a zero-branching semi-cell. Three stages are shown: at the onset of growth (figure 6a,d); during tip extension (figure 6b,e); and at the end of development, when the polar lobe has branched (figure 6c,f). Several species of *Micrasterias* have this degree of branching, including *M. arcuata*,

*M. pinnatifida*, *M. tropica* (figure 1h), *M. laticeps*, and some *M. truncata* and *M. radiata*. The arch-shaped polar lobes of *M. laticeps* and *M. truncata* will be discussed below in relation to single-branching species. Morphogenetically inactive ('dead') zones (in white) separate the peaks. In this computation, the value of  $k_p$  is low. This gives round lobe tips. The incipient obtuse-angled branching of the polar lobe (figure 6c) illustrates that, in this range of  $k_p$ , the model behaves much like the 'age effect' model of Harrison & Kolář (1988). Table 1 contains the parameters specific to this computation.  $k_p$  in the wings is lower than that in the polar lobe, to suppress wing branching.  $X_{th}$

Table 1. *Z*ero-branching parameters

$X_{th}$ , changing at (iterations)	0.0 (100 000) 0.1 (230 000) 1.2
$k_p$ (wing lobes)	12.22
$k_p$ (polar lobe)	13.0
$n_d$	1.0
$D_X$	125
$c_g$	2.0
iterations/growth step	500

becomes non-zero at the onset of growth (100 000 iterations) and shifts up late in the computation, to taper the lobes slightly and terminate growth.

### (b) *Single-branching wing lobes*

With singly branching wing lobes, the polar lobe and wings are of the same branching order. This is challenging to model, as the angles are always different in *Micrasterias* between pole and wings. A number of species normally have singly branching wings, including: some *M. radiata* (figure 7*e,f*); *M. americana*; some species of genus *Euastrum* (figure 7*g*); some *M. pinnatifida*; *M. truncata*; *M. decemdentata* (figure 7*h*); *M. depauperata*; and *M. jenneri*.

*M. radiata* (figures 7*e,f*) exemplifies well the problem of wing lobe versus polar lobe branching. Figure 7*a* is a computation featuring single wing lobe branching, but with an acute polar angle (though wider than the wings). Figure 7*b* has extensive arbitrary  $X_{th}$  shifting, but shows how this can greatly differentiate the polar angle and the wing angles. See table 2 for the parameters for all computations in figure 7. The  $X_{th}$  is initially high, forcing tip growth. It is relaxed to allow branching, but then forced up sharply to kill the new troughs at the tips. Because  $k_p$  is different in the pole and in the wings, the branching occurs at different rates. Such tight control of branching with  $X_{th}$  exaggerates these differences, leading to the very different branching angles.

Figure 7*c* has a morphology more like some *Euastrum* and *M. pinnatifida*: the wing lobes have wide clefts. The polar lobe is quite wide and again has a wider angle than the wings. In figure 7*d*, the arch-shaped polar lobe morphology of *M. truncata*, *M. suboblonga*, *M. depauperata*, some *M. pinnatifida*, and *M. decemdentata* (and some non-branchers) has been modelled. To do this, we took advantage of the ability to tune the morphogen peak shape with the parameter  $k_p$ . When  $k_p$  is high, as it is in the polar lobe in figure 7*d*, then the peaks are very square and tend not to split. Shifting of  $X_{th}$  was also used to allow continued growth of the small side lobes on the polar lobe.

### (c) *Two-branching wing lobes*

There are several species which display two branches in the wing lobes, including: some *M. radiata*; *M. radians* (figure 8*d*); and *M. crux-melitensis*. For the generation of two or more successive branches with acute angles, an alternating  $X_{th}$  is needed to switch between tip growth (high  $X_{th}$ ) and branching (low  $X_{th}$ ). In addition, there

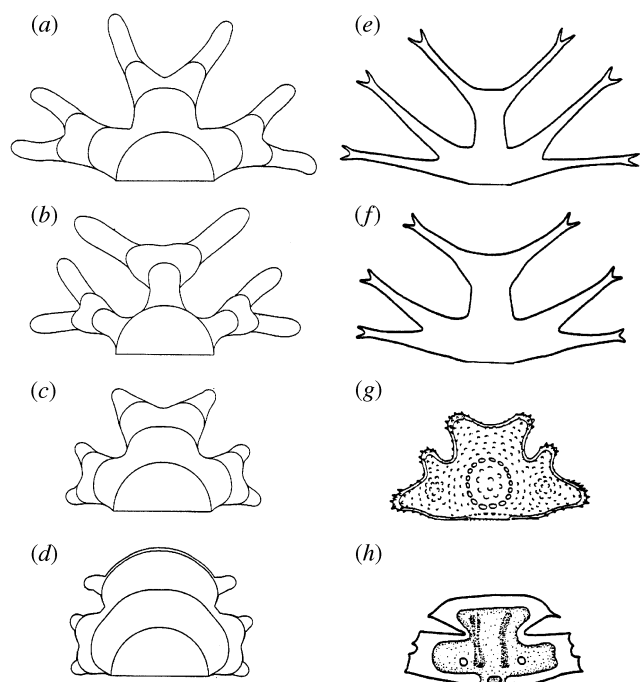


Figure 7. (*a-d*) Computed cell outlines at four stages of development for semi-cells with single branching in the wings, generating inner and outer wing lobes. Parameters: § 3a and table 2. (*e-h*) Fully formed semi-cell outlines from Prescott *et al.* (1977), with permission. (*e*) *M. radiata* var. *gracillima* f. *brevis*; (*f*) *M. radiata* var. *radiata* f. *radiata* (same as figure 2*c*); (*g*) *Euastrum verrucosum* var. *alatum* f. *floridense*; (*h*) *M. decemdentata*.

must be a decrease in spacing (§ 3c) to give the observed decrease in lobe size at higher branching number, and to avoid lobe overlap. Figure 8*a* has wide lobes and is like *M. radians* (figure 8*d*). For parameter values, see table 3.

The ‘craggy’, ill-defined cell outlines of some specimens of *M. crux-melitensis* and *M. americana* (figure 1*g*) appear to result from some loss of patterning information at about the initiation of the second branch. We attempted to model this by running the parameters of figure 8*a* with very rapidly decreasing diffusivities, as this tends to jumble the usual regularity of the Brusselator pattern. It proved too difficult to keep growth directed at all with this approach. This morphology is one that would be interesting to pursue.

### (d) *Three-branching wing lobes*

Many species exhibit three wing branchings, or more. These include *M. rotata* (figure 2*a,b*; figure 9*c*); *M. verrucosa* (figure 1*e*); *M. radiososa* (figure 8*e*); and *M. thomasi* (figure 1*a-d*). We have been able to generate such branching orders (figures 8*b* and 9*a*) by an additional shifting of  $X_{th}$  down, and then up, within the conditions for two-branchers, to give a third branching. At this stage, small errors from the grid and asymmetries of the chemical pattern have been so amplified that it is difficult to achieve similar angles in all tertiary branchings. A fourth branching would lead to lobe overlap from obtuse tertiary angles. We consider three-branchers to be our current limit on generating reasonably symmetrical cell outlines.

Table 2. *Single-branching parameters*

figure	$\tau_a$	$\tau_b$	$\tau_c$	$\tau_d$
cell outlines at (iterations)	100 000 180 000 280 000 620 000	100 000 240 000 340 000 660 000	100 000 160 000 220 000 360 000	100 000 160 000 200 000 370 000
$X_{th}$ , changing at (iterations)	0.0 (135 000) 0.1 (550 000) 0.2	0.0 (100 000) 0.05 (190 000) 0.01 (300 000) 0.08 (310 000) 0.2 (330 000) 0.05 (600 000) 0.15	0.0 (140 000) 0.05 (200 000) 0.125 (300 000) 0.2	0.0 (170 000) 0.075 (203 000) 2.5 (203 500) 0.075 (260 000) 0.25 (360 000) 2.0
$k_p$ (wing lobes)	18.0	17.1	17.28	17.01
$k_p$ (polar lobe)	18.36	18.0	18.0	18.36
$n_d$	4	8	4	1
$D_X$	50	50	50	50
$c_g$	1.0	0.5	0.5	0.5
iterations/growth step	1000	500	500	500

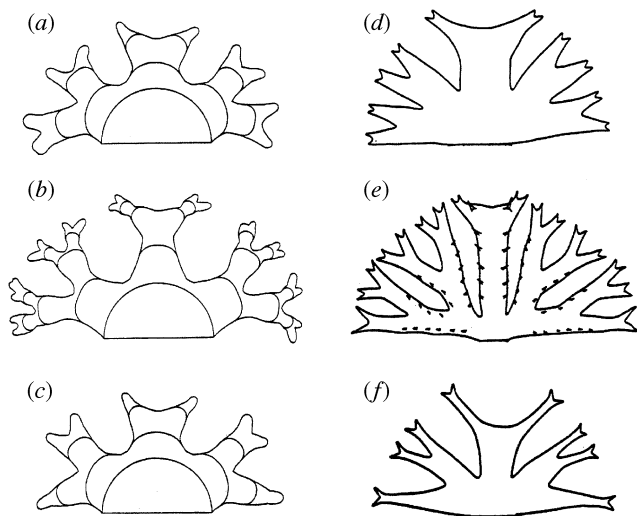


Figure 8. (a–c) Computed cell outlines at four stages of development for: (a) double-branching in the wings; (b) triple-branching in the wings; (c) abnormal development, outer wing lobes fail to branch, inner wing lobes branch. Parameters: § 3a and table 3. (c) has the same parameters as (a) except that one  $X_{th}$  shift is at 248 000 instead of 260 000 iterations. (d–f) Fully formed cell outlines from Prescott *et al.* (1977), with permission. (d) *M. radians*; (e) *M. radiosa* var. *murrayi* f. *elegantior*; (f) *M. radiata* var. *radiata* f. *radiata* (see also figures 2c and 7f). In the half-cell not shown, neither inner nor outer wing lobes branched.

Figure 8b is a computation of a relatively narrow-lobed three-branching semi-cell. Compare with *M. radiosa* (figure 8e). Figure 9a has fatter lobes (probably from a later initial  $X_{th}$  shift and lower  $n_d$ ) than figure 8b. The more continuous  $X_{th}$  shifting in figure 8b, in comparison with figure 9a (see table 3), results in less ‘pinching’ of the lobe sides at branch initiation. We cannot yet generate the

combination of fat lobes, smooth, straight lobe sides and repeated very narrow clefts seen in e.g. *M. rotata*, *M. thomasi* and *M. denticulata*.

In figure 9a, cell outlines are shown at equal time intervals of 20 000 iterations. Many more outlines appear in the wing lobes than the polar lobe, indicating that wing lobe growth has proceeded long after the ‘death’ of the polar lobe. This is somewhat unusual. It does not occur in any other computations shown in our figures.

Figure 9b,c shows an autoradiography pattern found by Lacalli (1973a, 1975; Lacalli & Harrison 1987) on cell-wall ghosts from cells treated with  $^3\text{H}$ -methylmethionine late in morphogenesis. It is thought to result from incorporation of the radiolabel into polysaccharides during primary cell-wall deposition, and to show a history of rapid growth regions during development. Compare these patterns with the red regions in figure 9a, showing the history of high  $X$  and hence rapid growth regions in our model. Figure 9d,e shows how similar our space–time picture of high  $X$  regions is to the actual patterns of seashell (*Conus marmoreus*) pigmentation markings and the computation of this pattern by Meinhardt (1995). Indeed, comparison of figures 9b,c and 9d,e encouraged us to build the feedback of equation (5) into the Brusselator. Meinhardt’s reaction–diffusion equations are dynamically quite different from the Brusselator (and might not generate symmetrical enough pattern for modelling of *Micrasterias*), but contain a feedback of one of the morphogens into one of its reactants that is key to getting fast tip death in our work and extinction of pigmentation in Meinhardt’s.

#### (e) *Abnormal development*

*Micrasterias* can miss branching events during development. Published pictures seem to suggest that this is quite common in *M. radiata*. See, for instance, figure 1f, in

Table 3. *Two- and three-branching parameters*

figure	8a	8b	9a
cell outlines at (iterations)	100 000 160 000 300 000 600 000	100 000 180 000 360 000 520 000 820 000	100 000 and every 20 000 iterations thereafter
$X_{th}$ , changing at (iterations)	0.0 (140 000) 0.075 (200 000) 0.01 (260 000) 0.075 (430 000) 0.0525 (560 000) 0.3	0.0 (130 000) 0.115 (198 000) 0.07 (240 000) 0.04 (280 000) 0.02 (315 000) 0.11 (400 000) 0.07 (430 000) 0.04 (450 000) 0.02 (515 000) 0.17 (600 000) 0.1	0.0 (140 000) 0.2 (180 000) 0.01 (265 000) 0.2 (340 000) 0.01 (465 000) 0.2
$k_p$ (wing lobes)	18.0	18.0	18.0
$k_p$ (polar lobe)	17.662	17.73	17.37
$n_d$	4	4	2
initial $D_X$	50	50	50
$c_g$	0.75	1.0	1.0
iterations/growth step	1000	1000	1000

which the upper wing lobes are branched in one semi-cell and unbranched in the other; and compare the branchings for the same variety in figures 7*f* and 8*f*. This type of irregularity is not difficult to simulate with our model. Figure 8*c* shows a computation with the same parameters as in figure 8*a*, but with the timing of one  $X_{th}$  shift slightly changed (see figure legend). From the model, we postulate that branching number anomalies can arise from slight errors in the timing of branching.

As stated in §3d, noise is added to the morphogen concentrations early in the computation, usually in the first 10 000 iterations. It is of interest to see how much noise the computations can take in the later stages before showing strong morphological changes. We found no significant morphological effects from adding continuous noise (for amplitude, see §3d) every 40th iteration throughout the computation. As we introduced such fluctuations more frequently, we began to see changes in shape. Both computations in figure 10 have the same parameters as that in figure 8*a*. All that has been altered is the frequency of noise additions: figure 10*a*, every 20th iteration; figure 10*b*, every tenth iteration. Both show morphological changes such as have been observed in *Micrasterias*. Figure 10*d* shows some *M. rotata* cells grown at elevated temperature. Figure 10*c* shows some cells from an ageing culture of *M. torreyi* (Lacalli 1973*a*). The sources of the developmental errors are clearly quite different in

these two cases, but we believe that both may correspond to excessive noise in chemical concentrations, as we have modelled in figure 10*a,b*.

## 5. DISCUSSION

### (a) *General features of the patterning dynamics*

Our modelling explores the possibility that branching tip growth in the genus *Micrasterias* is a manifestation of spatially patterned rates of membrane extension. This is in accord with the picture of vesicle fusion emerging from the experimental literature (§1). To accommodate the extra area, membrane extension must lead to outward movement of the membrane. For such displacement to become tip growth, there must be a rapidly growing region which is self-limiting in extent. And for branching tip growth, rapidly growing regions must multiply.

We assume that patterning of the rate of membrane extension occurs by activity within the membrane itself. There is evidence for patterned  $Ca^{2+}$  distribution on the membrane during morphogenesis both in *Micrasterias* (Meindl 1982) and in the dasyclad alga *Acetabularia* (Harrison *et al.* 1988). This supports our assumption that the patterning mechanism is chemical, which we have further assumed to be reaction–diffusion in the particular form of the Brusselator. These assumptions have enabled us to programme a model for computer experimentation.

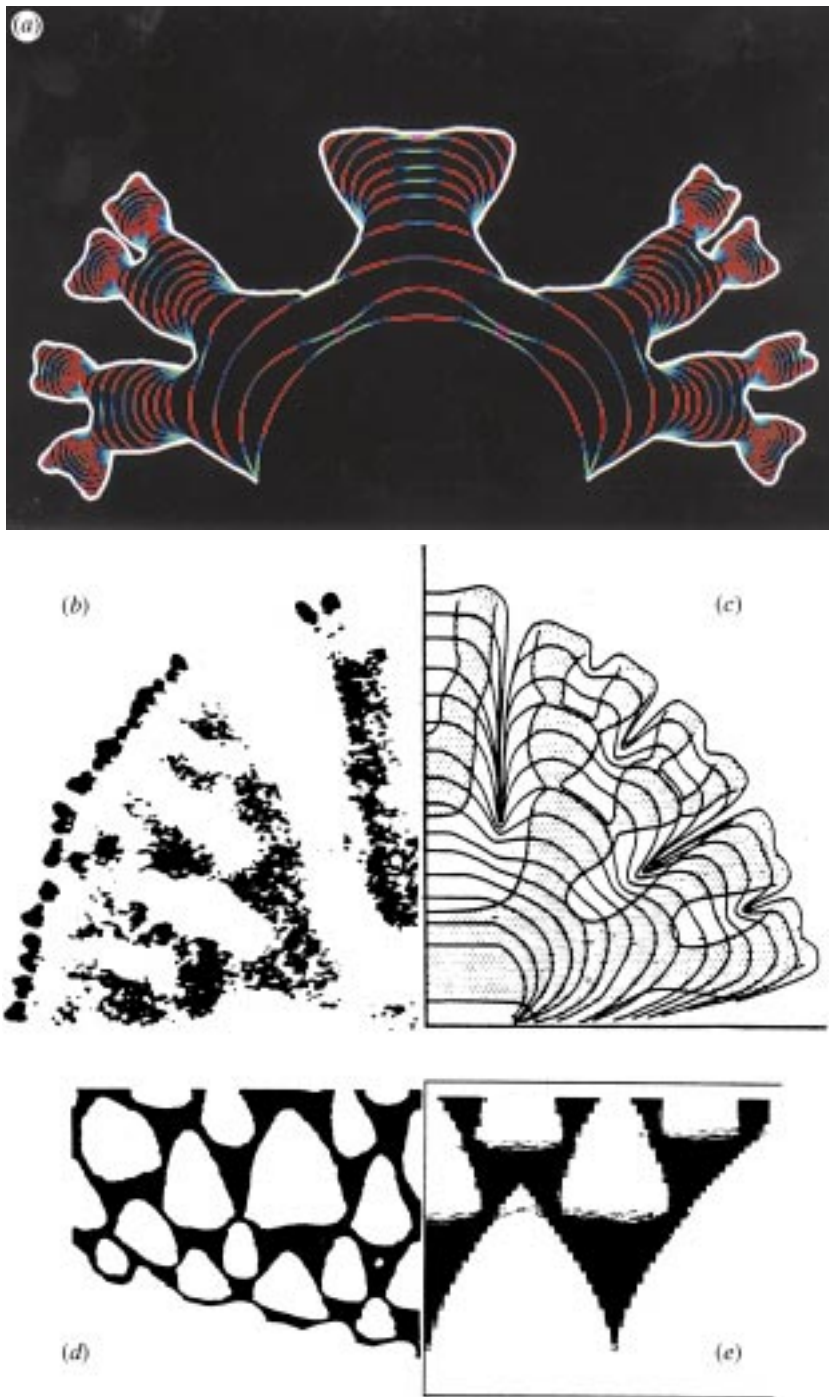


Figure 9. Time-space records of pattern-forming activity, computed and experimental. (a) Computed (this work) growth profiles equally spaced in time, colour-coded for  $X$  morphogen as in figure 6 (red is high). Parameters: § 3a and table 3. (b,c) Experimental, *M. rotata*, from Lacalli & Harrison (1987), with permission. Autoradiography of radiolabel incorporation into primary cell wall from  $^3\text{H}$ -methylmethionine near to the end of morphogenesis: (b) an autoradiograph; (c) tracing of autoradiographic pattern from more heavily labelled cell walls, superposed on growth profiles at 10 min intervals. See Lacalli (1975) for methodological details. (d,e) Pigmentation patterns of the seashell *Conus marmoreus*, experimental and computed, from Meinhardt (1995) with permission. (d) Experimental. (e) Computed by reaction-diffusion with additional features, among which the 'extinguishing reaction' is somewhat analogous to our feedback from  $X$  to  $A$ .

But we believe that our conclusions are more general than our assumptions.

We have advanced beyond the level reached by Harrison & Kolář (1988) by generating in computations: different degrees of branching in the polar and wing lobes; various degrees of wing lobe branching; acute branching angles, and different angles in polar and wing lobes; and some variations in lobe shape, from short and wide to long and narrow. All these features, however, are strongly controlled by the mechanism for self-limitation of the extent of a morphogenetic region, i.e. how such a region effectively pulls its boundary up after itself. Our general conclusion is that this apparently negative aspect of morphogenesis is crucial in governing species-specific cell architecture. The self-organizer of the cell morph-

ology is perhaps more of a self-sculptor than a self-creator.

The importance of growth termination, rather than growth, in control of morphogenesis, may not be intuitively obvious. But it is a common feature of pattern generation by dynamics. For reaction-diffusion, see Harrison (1993, especially chapter 6 and equation 6.30). For the Brusselator in particular, see table 9.1 in the same reference, in which the principal rate constant for emergence of pattern out of uniformity is  $k_1 = bB - d$  ( $b$ ,  $B$  and  $d$  are as in equations (1) of the present paper). Thus, pattern-forming ability is related to processes that destroy  $X$  (equations (1b) and (1d)), not to formation processes (equations (1a) and (1c)). Our chemical model does not contain an explanation for the existence of the

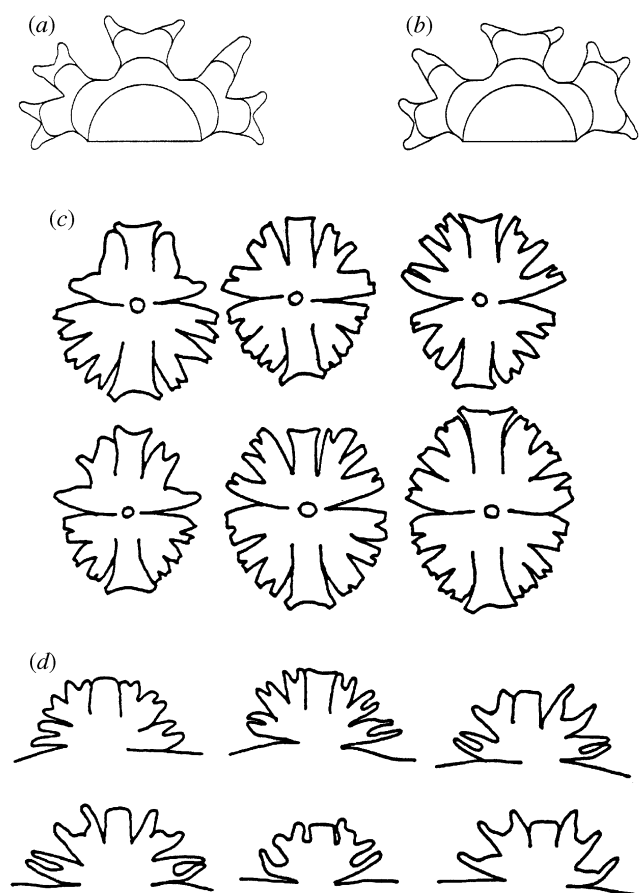


Figure 10. (a,b) Noise effects on the computations, when random input is used throughout the computations, not just in the first 10 000 iterations as in all other figures. Parameters as in figure 8a. With noise every 40 iterations, no change is seen from figure 8a. (a) Noise every 20 iterations; (b) noise every ten iterations. (c) Cells from a single ageing culture of *M. torreyi*. (d) *M. rotata* cells allowed to develop at a very high temperature (37.5 °C). (c) and (d) are from Lacalli (1973a) with permission.

threshold value  $X_{th}$  or the fast decay of  $X$  in the dead regions. We believe that the explanation must lie in  $X$ -dependences of the parameters  $b$ ,  $d$  and  $n_d$  unstated in our model. If  $b$  and  $d$  are controlled by enzyme activities, allosteric effects of  $X$  (activation of  $b$ , inhibition of  $d$ ) could be responsible if the effects reach saturation close to  $X_{th}$ . Although our model leaves these points to speculation, it is yet a substantial advance on the 'age effect' model of Harrison & Kolář (1988), both in extent of postulated chemical detail and in power to generate acute branching angles.

#### (b) Specific features of the modelling

For the many available reaction–diffusion models, we chose the Brusselator (equations (1) and (2)) because it is very efficient at generating periodic patterns. It produces new splittings of the patterns as a system grows, according to a wavelength predictable by linear analysis, even when the system is in nonlinear regions of dynamic behaviour (large peak amplitude or long time; see Harrison 1993, §9.1.5). This choice of model is not necessarily unique. All discussion based on rate constants of the model is subject to later modification if enough infor-

mation emerges to identify the nature of the dynamics more precisely.

For instance, morphogen peaks tend not to respond to growth by splitting if they have become very square (§3c). This behaviour is quite uncharacteristic of the Brusselator without our modifications (Harrison 1993) but resembles the behaviour of the hyperchirality model (Harrison & Lacalli 1978). The latter was discussed in relation to morphogenesis of *M. rotata*, because of the model's tendency to give square peaks. We tried the hyperchirality model in the present work, but found the modified Brusselator much more versatile for giving an account of interspecies variation of shape.

The parameter  $k_p$  in equation (5) allows 'tuning' of the shape of the  $X$  catalyst peaks. Low  $k_p$  leads to obtuse branching angles; higher  $k_p$  gives square peaks which lead to acute branching angles. Very high  $k_p$  was used to take advantage of this feature of the model in generating the arch-shaped polar lobe in figure 7d. Acute angles require also, however, the continued, or even increased, decay of  $X$  in the non-morphogenetic, boundary regions, with diffusive communication throughout the surface. This provides a 'drain' on the morphogenetic regions which tends to keep the  $X$  peaks close together during the branching process. In addition, since our evaluation for loss of morphogenetic ability (and implementation of equations (6)) is based on a threshold value of  $X$ , there is a fast morphological response to  $X$  peak splitting.

The parameters in the model are tightly constrained by the need to make acute-angled branches. Because of their interdependency, it is difficult to vary further any of the parameters to provide for species specific features. Independent variables have been added to the model (§3c) to address certain of these features: spatial variation of  $k_p$  to generate the wing–pole difference in branching order and branching angle; shifting of  $X_{th}$  timing for specific morphological features, and higher order acute-angled branching; and decrease of diffusivities to account for the decrease in spacing for higher branching species.

Only spatial variation of  $k_p$  has been used in all of the computations. Lower (zero and one) branching computations do not require spacing decrease, and  $X_{th}$  shifting has only been used to terminate growth in figures 6 and 7a. In figure 7c,  $X_{th}$  is raised mid-computation to taper the lobes. In the remaining two low-branching computations, figure 7b,d,  $X_{th}$  shifting has been extensive, to increase the effect of the  $k_p$  differences between the polar lobe and the wing lobes. For higher (two and three) branching computations, spacing decrease is used to avoid lobe overlap, and the  $X_{th}$  is alternated between high and low to give successive acute-angled branchings. With fixed  $X_{th}$ , only the first branching can be acute; all others will be obtuse. It was shown, with two- and three-branchers, that more gradual shifting of  $X_{th}$  led to smoother lobe sides. This suggests that the boundary-control mechanism in *Micrasterias* might have a more continuous shifting. In the computations, however, the sensitivity of the morphology to the timing of the  $X_{th}$  shifting precludes easy development of a dynamically generated function for the shifting.

These three factors have been added externally to the model, and do not currently have a dynamical basis, i.e. they are not generated by a system of equations, as is the

chemical pattern. We were led to add these factors in order to generate certain features of *Micrasterias*. They point towards a larger-scale cellular dynamics to be integrated with membrane-localized growth and pattern formation for a more complete model. We have used specific points of the chemical model at which to impose these external features; but they are much more general. For instance, variation in dynamics between the polar and the wing lobes may not be spatial variation in the rate constant  $k_p$  controlling  $X$  feedback on to  $A$ . But our modelling has shown the important feature that a variation of a few per cent in some dynamic parameter between the polar lobe and the wing lobes can generate their difference in branching behaviour. This may stem from pattern-forming events during septum formation; see Lacalli (1973*b*) for details on this process. Likewise,  $X_{th}$  shifting may not be the true mechanism switching between branching and tip growth. But it points to the importance of feedback of the chemical patterning mechanism on to its boundaries with the right time-scale to give successive acute-angled branches. Finally, we have used diffusivity decrease for spacing decrease. Even if our Brusselator model is exactly the right one, it affords a choice among eight parameters that quantitatively determine its wavelength.

#### (c) *Genetics, non-genetic templates and epigenesis*

One of our major long-term goals is to develop a model to the point that we can begin to understand how interspecific genetic variation leads to morphological variation through changes in chemical rates. There are several remaining hurdles to this, however, both from the biology and from the model. Biologically, there is some difficulty in distinguishing between genetic and cellular factors in a given cell's morphology. It is known that anucleate cells are able to produce the initial three-lobe pattern, but nothing more (reviewed in Kallio & Lehtonen 1981). The presence of the nucleus is required for branching and full development. So, there is a definite genetic influence on morphology. However, it is not uncommon for a daughter semi-cell to miss a branching event and have a quite different morphology from the parent semi-cell; enough that the daughter may look closer to a different species. In addition, the taxonomy of *Micrasterias* is problematic with regard to morphology: species are not always distinguished along clear distinctions in shape. Finally, there appear to be non-genetic forms of inheritance in *Micrasterias*. For instance, Lacalli (1976) has proposed a geometrical influence from the adult semi-cell on the early pattern formation of the daughter semi-cell. As well, there is a uniradiate form of *M. thomasi* (Waris 1950), in which one wing lobe does not form, and which is maintainable over multiple generations of asexual division. Such a defect may not be genetically based. Morphological features that are maintained within given species (albeit with some defective cells) include lobe length, lobe width, branching angles and branching number. These would appear to be associated with the genome of the given species. Genes produce chemicals, though, and not their patterned localization. A pattern-forming mechanism is necessary for morphogenesis; and that mechanism must be chemical at some level in order to interact with the genome.

In our model, one of the chief parameters for controlling branching is the value of  $X_{th}$ . Threshold cut-offs (of more than one kind) to morphogenesis do exist in chemical pattern formation (see Harrison 1993, §§ 6.4.1, 7.2, 7.3 and 9.1.3). The need, in the present stage of our modelling, for timing of  $X_{th}$  shifting in higher-order branching suggests that some changes, perhaps initiated and therefore timed in the interior of the cell, are affecting processes controlled by  $X$ . Such intracellular control of our membrane-orientated model may be a major component of the nuclear control of morphogenesis (i.e. the necessity of the nucleus for branching), and therefore be closely tied to interspecific variation.

We suppose  $X$  to be a membrane protein, associated with vesicle fusion (as in Kiermayer & Meindl 1989). We speculate (as also Harrison *et al.* (1997), for a similar morphogen system that may be at work in *Acetabularia*), that  $X$  might be some sort of autophosphorylating kinase, with  $A$  its unphosphorylated form. This protein may be Ca-binding (Kiermayer & Meindl 1989), with this binding perhaps activating the phosphorylation process (Harrison *et al.* 1997). In such a scenario, the feedback of the membrane on the genome (represented in the model by  $X_{th}$ ) may be through some type of signal transduction pathway. The threshold may represent the level of  $X$  below which the membrane-genome communication necessary for maintenance of growth ceases and the decay of  $X$  increases. Timed events at the genome or within the cell could control the  $X$ -value at which this communication cuts off.

In attempting to model a process such as *Micrasterias* morphogenesis, a question of simplicity versus complexity arises. On the one hand, we have tried to keep the model as simple as possible. We have used a simple model (chemical pattern generator and the means for that pattern to be translated into surface growth) with quite complex behaviour, arising from feedbacks both between growth and chemistry and within the chemistry. We do not wish to deny the complexity of *Micrasterias* molecular biology with the simple set of reactions set forth in § 3. What we have done is to follow a traditional physico-chemical method of seeking the few reactions which contain the essential dynamics of an overall reaction process. (Some of the simplest inorganic reactions contain as many as 30 steps, but only a handful of these determine the kinetics of the system.) In the simplest cases, these essential reactions may capture the overall dynamics by being rate-limiting, rendering faster reactions dynamically unimportant. In more interesting cases, intermediate steps may allow such behaviour as pattern formation, as in the present model. The reactions set forth in § 3 may be easily considered as part of a larger biochemical system: indeed, single variables in those reactions may be simplifications of multiple binding events.

#### (d) *Future work*

Probably the most significant general conclusion from our modelling is the importance of the loss ('death') of pattern-forming ability in the slow-growing regions that become clefts between lobes. This should be considered in relation to the generation of any multilobed system, not only in unicellular algae but also at apical meristems and

growing edges of structures in multicellular plants; and not only in plants, but also in the animal kingdom, in the genesis of multilobed glands, lungs and perhaps even limbs. For multicellular organogenesis, the topic is clearly related to the consequences for shape development of programmed cell death or exit from the cell cycle. Some of the general framework of our modelling might be used with advantage in any of these fields.

For example, in a recent review of wing and leg morphogenesis in *Drosophila*, Serrano & O'Farrell (1997), the authors raise the question which is the general topic of the present paper, as also of Harrison & Kolář (1988), in the words: 'One of the most mysterious features of morphogenesis is that structures form themselves as they grow... How are the actions of morphogens coordinated with the process of growth?'

In all work that seeks to answer this question by postulating putative chemical interactions of the morphogens and analysing the dynamics of these interactions, it is desirable that every necessary reaction step should be explicitly stated. We have done this in the present work for the Brusselator pattern-forming mechanism and for part of the switch-off mechanism in slow-growing regions, the feedback from *X* to *A*. But our model falls short of this ideal in relation to the threshold value for switch-off,  $X_{th}$ . To make this part of the model less arbitrary and more explicit chemical-kinetically, one must be able to cope with a switching which is not to zero growth ('death') but to slow unpatterned growth. To do this (see § 2b), it is necessary to treat the growth at saddle points (clefs) properly by performing 3D computations. Our immediate intention is therefore to pursue 3D modelling of *Micrasterias*. We hope not only to fine-tune our ability to generate the shapes found within this genus, but also to establish a general framework for chemical, mathematical and computational modelling of the growth of multilobed structures.

We thank John Hogg and Paul Hilchey for help with the colour-mapping and keeping our computer system running, respectively. This project was supported by NSERC operating and equipment (workstation) grants. We would also like to thank Thurston Lacalli for helpful suggestions on the manuscript.

## REFERENCES

- Bathey, N. H. & Blackbourn, H. D. 1993 The control of exocytosis in plant cells. *New Phytol.* **125**, 307–338.
- Couté, A. & Tell, G. 1981 *Ultrastructure de la paroi cellulaire des Desmidiacées au microscope électronique à balayage*. Vaduz: J. Kramer.
- Denet, B. 1996 Numerical simulation of cellular tip growth. *Phys. Rev. E* **53**, 986–992.
- Giddings, T. H., Brower, D. L. & Staehelin, L. A. 1980 Visualization of particle complexes in the plasma membrane of *Micrasterias denticulata* associated with the formation of cellulose fibrils in primary and secondary cell walls. *J. Cell Biol.* **84**, 327–339.
- Gratzl, M. 1980 Transport of membranes and vesicle contents during exocytosis. In *Biological chemistry of organelle formation* (ed. T. Bücher, W. Seebald & H. Weiss), pp. 165–174. Berlin, Heidelberg and New York: Springer.
- Green, P. B. 1994 Connecting gene and hormone action to form, pattern and organogenesis: biophysical transductions. *J. Exp. Bot.* **45**, 1775–1788.

- Green, P. B. & King, A. 1966 A mechanism for the origin of specifically oriented textures in development with special reference to *Nitella* wall texture. *Aust. J. Biol. Sci.* **19**, 421–437.
- Harold, F. M. 1990 To shape a cell: an inquiry into the causes of morphogenesis of microorganisms. *Microbiol. Rev.* **54**, 381–431.
- Harold, F. M., Harold, R. L. & Money, N. P. 1995 What forces drive cell wall expansion? *Can. J. Bot.* **73** (Suppl. 1), S379–S383.
- Harrison, L. G. 1992 Reaction–diffusion theory and intracellular differentiation. *Int. J. Plant Sci.* **153**, S76–S85.
- Harrison, L. G. 1993 *Kinetic theory of living pattern*. New York and Cambridge: Cambridge University Press.
- Harrison, L. G. 1994 Kinetic theory of living pattern. *Endeavour* **18**, 130–136.
- Harrison, L. G. & Kolář, M. 1988 Coupling between reaction–diffusion prepattern and expressed morphogenesis, applied to desmids and dasyclads. *J. Theor. Biol.* **130**, 493–515.
- Harrison, L. G. & Lacalli, T. C. 1978 Hyperchirality: a mathematically convenient and biochemically possible model for the kinetics of morphogenesis. *Proc. R. Soc. Lond. B* **202**, 361–397.
- Harrison, L. G. & Lacalli, T. C. 1993 Controversy over concepts: long-range communication versus 'no crosstalk'. In *Oscillations and morphogenesis* (ed. L. Rensing), pp. 43–56. New York, Basel, Hong Kong: Marcel Dekker.
- Harrison, L. G., Graham, K. T. & Lakowski, B. C. 1988 Calcium localization during *Acetabularia* whorl formation: evidence supporting a two-stage hierarchical mechanism. *Development* **104**, 255–262.
- Harrison, L. G., Snell, J., Verdi, R., Vogt, D. E., Zeiss, G. D. & Green, B. R. 1981 Hair morphogenesis in *Acetabularia mediterranea*: temperature-dependent spacing and models of morphogen waves. *Protoplasma* **106**, 211–221.
- Harrison, L. G., Donaldson, G., Lau, W., Lee, M., Lin, B. P., Lohachitrant, S., Setyawati, I. & Yue, J. 1997 CaEGTA uncompetitively inhibits calcium activation of whorl morphogenesis in *Acetabularia*. *Protoplasma* **196**, 190–196.
- Hoftberger, M., Url, T. & Meindl, U. 1995 Disturbance of the secretory pathway in *Micrasterias denticulata* by tunicamycin and cyclopiazonic acid. *Protoplasma* **189**, 173–179.
- Holloway, D. M. & Harrison, L. G. 1995 Order and localization in reaction–diffusion pattern. *Physica A* **222**, 210–233.
- Holzinger, A., Callaham, D. A., Hepler, P. K. & Meindl, U. 1995 Free calcium in *Micrasterias*: local gradients are not detected in growing lobes. *Eur. J. Cell Biol.* **67**, 363–371.
- Kallio, P. & Lehtonen, J. 1981 Nuclear control of morphogenesis in *Micrasterias*. In *Cytomorphogenesis in plants* (ed. O. Kiermayer), pp. 191–214. Wien and New York: Springer.
- Kiermayer, O. 1964 Untersuchungen über die Morphogenese und Zellwandbildung bei *Micrasterias denticulata* Bréb. *Protoplasma* **59**, 382–420.
- Kiermayer, O. 1967 Das Septum-Initialmuster von *Micrasterias denticulata* und seine Bildung. *Protoplasma* **64**, 481–484.
- Kiermayer, O. 1968 Hemmung der Kern- und Chloroplastenmigration von *Micrasterias* durch Colchicin. *Naturwissenschaften* **55**, 299–300.
- Kiermayer, O. 1970a Causal aspects of cytomorphogenesis in *Micrasterias*. *Ann. NY Acad. Sci.* **175**, 686–701.
- Kiermayer, O. 1970b Elektronenmikroskopische Untersuchungen zum Problem der Cytomorphogenese von *Micrasterias denticulata* Bréb. I. Allgemeiner Überblick. *Protoplasma* **69**, 97–132.
- Kiermayer, O. 1981 Cytoplasmic basis of morphogenesis in *Micrasterias*. In *Cytomorphogenesis in plants* (ed. O. Kiermayer), pp. 147–190. Wien and New York: Springer.
- Kiermayer, O. & Meindl, U. 1989 Cellular morphogenesis: the desmid (chlorophyceae) system. In *Algae as experimental systems* (ed. A. W. Coleman, L. J. Goff & J. R. Stein-Taylor), pp. 149–167. New York: Alan R. Liss.

- Lacalli, T. C. 1973a Morphogenesis in *Micrasterias*. PhD thesis, University of British Columbia.
- Lacalli, T. C. 1973b Cytokinesis in *Micrasterias rotata*. *Protoplasma* **78**, 433–442.
- Lacalli, T. C. 1975 Morphogenesis in *Micrasterias*. I. Tip growth. II. Patterns of morphogenesis. *J. Embryol. Exp. Morphol.* **33**, 95–116, 117–127.
- Lacalli, T. C. 1976 Morphogenesis in *Micrasterias*. III. The morphogenetic template. *Protoplasma* **88**, 133–146.
- Lacalli, T. C. & Harrison, L. G. 1987 Turing's model and branching tip growth: relation of time and spatial scales in morphogenesis, with application to *Micrasterias*. *Can. J. Bot.* **65**, 1308–1319.
- Lehtonen, J. 1984 The significance of  $\text{Ca}^{2+}$  in the morphogenesis of *Micrasterias* studied with EGTA, Verapamil,  $\text{LaCl}_3$  and calcium ionophore A23187. *Plant Sci. Lett.* **33**, 53–60.
- McNally, J. G., Cowan, J. D. & Swift, H. 1983 The effects of the ionophore A23187 on pattern formation in the alga *Micrasterias*. *Dev. Biol.* **97**, 137–145.
- Meindl, U. 1982 Local accumulations of membrane associated calcium according to cell pattern formation in *Micrasterias denticulata*, visualized by chlorotetracycline fluorescence. *Protoplasma* **110**, 143–146.
- Meinhardt, H. 1995 *The algorithmic beauty of seashells*. Berlin, Heidelberg, New York: Springer.
- Prescott, G. W., Croasdale, H. T. & Vinyard, W. C. 1977 *A synopsis of North American desmids. II. Desmidiaceae: Placodermatae, section 2*. Lincoln and London: University of Nebraska Press.
- Prigogine, I. & Lefever, R. 1968 Symmetry-breaking instabilities in dissipative systems. II. *J. Chem. Phys.* **48**, 1695–1700.
- Scagel, R. F., Bandoni, R. J., Maze, J. R., Rouse, G. E., Schofield, W. B. & Stein, J. R. 1982 *Nonvascular plants: an evolutionary survey*. Belmont, CA: Wadsworth Publishing Co.
- Serrano, N. & O'Farrell, P. H. 1997 Limb morphogenesis: connections between patterning and growth. *Curr. Biol.* **7**, R186–R195.
- Sel'kov, E. E. 1968 Self-oscillations in glycolysis. I. A simple kinetic model. *Eur. J. Biochem.* **4**, 79–86.
- Staehein, A. & Giddings, T. H. 1982 Membrane-mediated control of cell wall microfibrillar order. In *Developmental order: its origin and regulation* (ed. S. Subtelny & P. B. Green), pp. 133–147. New York: Alan R. Liss.
- Steer, M. W. 1988 The role of calcium in exocytosis and endocytosis in plant cells. *Physiologia Pl.* **72**, 213–220.
- Steer, M. W. & Steer, J. M. 1989 Pollen tube tip growth. *New Phytol.* **111**, 323–358.
- Tippit, D. H. & Pickett-Heaps, J. D. 1974 Experimental investigations into morphogenesis in *Micrasterias*. *Protoplasma* **81**, 271–296.
- Troxell, C. L. 1989 Transcellular ionic currents during primary wall morphogenesis in *Micrasterias* and *Closterium*. *Biol. Bull.* **176** (Suppl.), 36–40.
- Troxell, C. L. & Scheffey, C. 1991 Ionic currents flow through *Micrasterias* and *Closterium* cells during expansion of the primary cell wall. *Planta* **184**, 218–225.
- Troxell, C. L., Scheffey, C. & Pickett-Heaps, J. D. 1986 Ionic currents during wall morphogenesis in *Micrasterias* and *Closterium*. In *Ionic currents in development* (ed. R. Nuccitelli), pp. 105–112. New York: Alan R. Liss.
- Turing, A. M. 1952 The chemical basis of morphogenesis. *Phil. Trans. R. Soc. Lond. B* **237**, 37–72.
- Tyson, J. J. & Kauffman, S. A. 1975 Control of mitosis by a continuous biochemical oscillation. *J. Math. Biol.* **1**, 289–310.
- Tyson, J. J. & Light, J. C. 1973 Properties of two-component bimolecular and trimolecular chemical reaction systems. *J. Chem. Phys.* **59**, 4164–4173.
- Ueda, K. & Noguchi, T. 1988 Microfilament bundles of F-actin and cytomorphogenesis in the green alga *Micrasterias crux-melitensis*. *Eur. J. Cell Biol.* **46**, 61–67.
- Ueda, K. & Yoshioka, S. 1976 Cell wall development of *Micrasterias americana*, especially in isotonic and hypertonic solutions. *J. Cell Sci.* **21**, 617–631.
- Waris, H. 1950 Cytophysiological studies on *Micrasterias*. II. The cytoplasmic framework and its mutation. *Physiol. Plant.* **3**, 236–246.
- West, W. & West, G. S. 1905 *A monograph of the British Desmidiaceae*, vol. 2. London: Adlard & Son, for the Ray Society.

